Theoretical Study of H^+ Translocation along a Model Proton Wire

Régis Pomès and Benoît Roux*

Groupe de Recherche en Transport Membranaire (GRTM), Departments of Physics and Chemistry, Université de Montréal, Case Postale 6128, Succ. Centre-Ville, Montréal, Québec, Canada H3C 3J7

Received: September 1, 1995; In Final Form: November 16, 1995[⊗]

The mechanism of proton translocation along linear hydrogen-bonded water chains is investigated. Classical and discretized Feynman path integral molecular dynamics simulations are performed on protonated linear chains of 4, 5, and 9 water molecules. The dissociable and polarizable water model PM6 of Stillinger and co-workers is used to represent the potential energy surface of the systems. The simulations show that quantum and thermal effects are both important because the height of the barriers opposing proton transfer are strongly coupled to the configuration of the chain, which is, in turn, affected by the presence of an excess proton. For characterization of the quantum effects, the energy levels of the hydrogen nucleus located at the center of a protonated tetrameric water chain are calculated by solving the Schroedinger equation for an ensemble of configurations which were generated with path integral simulations. Analysis shows that the first excitation energies are significantly larger than the thermal energy k_BT and that quantum effects are dominated by the zero-point energy of the proton. The quantum correlations between the different proton nuclei are found to be negligibly small, suggesting that an effective one-particle description could be valid. Potential of mean force surfaces for proton motion in relation to the donor−acceptor separation are calculated with classical and path integral simulations for tetrameric and pentameric water chains. The mechanism for long-range proton transfer is illustrated with a simulation of a hydrogen-bonded chain of nine water molecules. During the simulation, cooperative fluctuations which modulate the asymmetry of the chain enable the spontaneous translocation of protons over half of the length of the chain.

Introduction

Processes involving the rapid translocation of hydrogen ions over long distances are required for the establishment of proton electrochemical potential gradients across biological membranes, which is essential to the proper function of the energy-transducing membrane.[1] Understanding how specific macromolecular protein assemblies perform this complex function is a central question in biology and in biophysics. In a number of well-characterized systems,[2−4] there is growing evidence for the presence of water molecules embedded in the interior of the protein matrix where they could play an important functional role. In particular, a chain of 14 water molecules extending over 23 Å from the interior of the protein to the cytoplasmic side has recently been observed in the crystallographic X-ray structure of the photosynthetic reaction center (PRC) of *Rhodobacter sphaeroides*.[3] Similarly, refinement of the X-ray structure of the lumen-side domain of cytochrome *f* (Cyt*f*) reveals the presence of a chain of 5 water molecules, 4 of which form a linear pathway extending 12 Å from the interior of the protein to the bulk solvent.[4] Lastly, contrast neutron diffraction studies indicate that 4 water molecules are trapped in the neighborhood of the Schiff base in bacteriorhodopsin of *Halobacterium* (bR).[5] Although the current three-dimensional structure from electron crystallography lacks sufficient resolution to locate water molecules,[6] computer modelization indicates that these water molecules could form a linear chain in a narrow nonpolar region of the protein, between the intracellular surface and the Schiff base.[7] The location of such chains of water molecules in the protein structure suggests that they might participate in proton translocation. For example, the water chains observed in the Cyt*f* and the reaction center structures could be implicated respectively in H^+ extrusion from the *b*6*f* complex or the reprotonation of the secondary quinone Q_B.[4] Furthermore, experimental evidence indicates that water molecules trapped in the bR structure are essential for the reprotonation step, requiring the translocation of a proton over a distance of 10−12 Å from Asp 96 to the Schiff base at the end of the photocycle.[2]

Because they are thought to be particularly effective in mediating the translocation of protons, such hydrogen-bonded water chains have been called *proton wires*.[8] Perhaps, the simple transmembrane ion channel formed by the pentadecapeptide gramicidin A provides one of the most striking illustrations of the high proton mobility along hydrogen-bonded water chains.[9] In the membrane, the gramicidin A molecule forms a helical channel of about 26 Å in length and 4 Å in diameter; its structure is such that the permeation process must involve the single file movement of a partially dehydrated ion and water through the interior of a narrow pore.[9,10] However, analysis of electrical conductance and flux data has lead to the remarkable conclusion that protons diffuse effectively faster than the water molecules arranged in single file along the channel.[9] In other words, the dominant mechanism responsible for the proton conductance is not the diffusion of the hydronium species, OH_3^+, through the gramicidin channel.

Instead, the high mobility of H^+ in proton wires is thought to arise from successive protonation−dissociation reactions, whereby hydrogen ions hop from oxygen to oxygen along the hydrogen-bonded chain, in a Grotthuss-like mechanism.[11] However, even in the case of the relatively simple and well-characterized gramicidin channel,[9,12] experimental elucidation of the molecular mechanism is difficult because it is intrinsically transient in nature. Theoretical methods represent a possible approach for exploring the microscopic processes underlying proton transport in such complex systems. Due to their importance in chemistry and biology, much work has been

* Author to whom correspondence should be addressed.
[⊗] Abstract published in *Advance ACS Abstracts,* January 15, 1996.

0022-3654/96/20100-2519$12.00/0

devoted to the study of proton transfer phenomena (see ref 13 for a recent discussion). For investigation of the particular influence of various factors, such as the variations of the barrier height between the donor and acceptor or the external forces due to the surrounding solvent, proton transfer processes have traditionally been characterized on the basis of simple model systems depicting a H^+ shared by two atomic centers representing the donor−acceptor pair.[14,15] Despite their interest, such models do not constitute a realistic description of proton transfer in a protic medium and stop short of providing a basis for understanding the function of proton wires.[16−18]

For a meaningful investigation of proton translocation along proton wires, it is necessary to allow full flexibility and dissociation of the water molecules. Particularly in the case of protonated water aggregates, it may be essential to take into account the inherently collective nature of the proton transfer which results from the equivalence of all potential donor and acceptor molecules in a protic medium. In such systems, the notion of solvent cooperativity reaches its full meaning, which suggests that all the water molecules of the system should be treated on the same footing. In addition, the proton translocation process being essentially governed by thermal motions, it is necessary to incorporate the influence of thermal fluctuations corresponding to a finite temperature in a quantum statistical mechanical formulation. *Ab initio* quantum chemistry represent the most fundamental approach for calculating the Born−Oppenheimer potential energy surface of the system. Yet, at the present time this requirement is difficult to meet with high-level *ab initio* calculations. The accurate computation of the properties of protonated water clusters is difficult because of the strong anharmonicity of the potential energy surface governing the motion of the nuclei.[19,20] Recently, a molecular dynamics simulation of a hydronium ion in aqueous solution using forces computed directly from density functional theory (DFT) has been reported.[21] However, the dynamical trajectory was generated using the classical equation of motion, and the quantum effects due to the light mass of hydrogen nuclei were neglected. An effective method to incorporate quantum effects in many-body systems consists of using discretized Feynman path integral simulations.[22] Although the approach has usually been employed to investigate proton transfer with model interaction potentials.[23−25] its incorporation into an all-quantum molecular dynamics simulation method (AQMD) was recently presented in the case of small proton hydrates, OH_3^+ and $O_2H_5^+$.[26] In that study, path integral simulations were performed using an *ab initio* Born−Oppenheimer potential energy surface calculated using local DFT. Such a rigorous treatment remains computationally prohibitive in the case of large biological systems. Alternative approaches may be sought in the study of the essential factors governing the translocation of a proton in a realistic, yet computationally tractable, model of a proton wire. In an earlier paper,[27] we presented classical and path integral computer simulations of a model proton wire of 4 water molecules. The polarizable and dissociable PM6 potential energy function for water developed by Stillinger and co-workers was used.[28−30] In particular, the study revealed that the quantum dispersion of the hydrogen nuclei had a significant influence on the conformational fluctuations of the sytem at 300 K. Configurations in which the energy profile of the central proton along the transfer coordinate possessed a single- or double-well character occurred spontaneously due to thermal fluctuations.[27]

The goal of the present work is to pursue our investigation of the dominant structural and dynamical features of proton wires and to assess the importance of quantum effects, such as tunneling and zero point vibration. Following the spirit of our preliminary study, we limit the simulations to protonated chains of hydrogen-bonded water molecules in vacuo as relatively simple models of proton wires. We point out that the study of the mechanism of proton wires in vacuo opens the way to simulations of proton translocation in biological systems.[31] Linear chains of 4, 5, and 9 water molecules are studied here. These numbers correspond approximately to the proposed length of the proton wires of bR,[5,7] the cytochrome *b6f* complex,[4] and the gramicidin channel.[9,10] A description of the model and of the methodology used to compute molecular dynamics simulations is presented, and the potential energy dependence on the donor−acceptor distance is briefly discussed. The properties of a protonated chain of 4 water molecules, $O_4H_9^+$, are then investigated. The quantum energy levels of the central proton are calculated, and the importance of quantum correlations between the hydrogen nuclei is assessed. The potential of mean force surfaces for the motion of a proton in relation to oxygen−oxygen separations are subsequently presented and compared for chains of 4 and 5 water molecules. Finally, the mechanism for long-range proton transfer along a proton wire is illustrated in the case of the hydrogen-bonded chain of 9 water molecules.

Method

Potential Energy Function. The PM6 version of the polarization model developed by Stillinger and co-workers[28−30] was used to approximate the potential energy surface of protonated water chains. The PM6 model energy function was developed and parametrized to accurately reproduce the structure and energy of small hydrogen-bonded cationic and anionic water clusters. In contrast with rigid[32,33] or partially flexible water models,[34] the basic structural elements of PM6 are H^+ and O^{2-} atoms, a feature which makes it possible to account for the full dissociation of water molecules into ionic fragments. For a configuration of the oxygen and hydrogen constituents with coordinates $\{\mathbf{r}_O\} = \{\mathbf{r}_{O_1}, ..., \mathbf{r}_{O_{N_O}}\}$ and $\{\mathbf{r}_H\} = \{\mathbf{r}_{H_1}, ..., \mathbf{r}_{H_{N_H}}\}$, the PM6 potential energy is[28]

$$U(\{\mathbf{r}_O\},\{\mathbf{r}_H\}) = \sum_{i<j=1}^{N_O} \phi_{OO}(|\mathbf{r}_{O_i} - \mathbf{r}_{O_j}|) + \sum_{i=1}^{N_O}\sum_{j=1}^{N_H} \phi_{OH}(|\mathbf{r}_{O_i} - \mathbf{r}_{H_j}|) + \sum_{i<j=1}^{N_H} \phi_{HH}(|\mathbf{r}_{H_i} - \mathbf{r}_{H_j}|) + \Phi_{pol}(\{\mathbf{r}_O\},\{\mathbf{r}_H\}) \quad (1)$$

where ϕ_{OO}, ϕ_{OH}, and ϕ_{HH} are pairwise radially symmetric functions and Φ_{pol} represents a many-body polarization energy contribution resulting from the polarization of the oxygen nuclei.

In order to illustrate the properties of the PM6 model for the transfer of a hydrogen ion between two water molecules (i.e., in the $H_2O-(H^+)-OH_2$ complex), the dependence of the potential energy profile upon the oxygen−oxygen separation is described and compared with the results of *ab initio* calculations. The *ab initio* calculations were performed at the Hartree−Fock level with the 4-31G basis set using the GAUSSIAN90 program.[35] The 4-31G basis set was found to be satisfactory by previous authors,[36] although the difficulty in calculating the accurate structures and energy in the case of small water clusters is documented.[37] At this level, the optimized geometry of $O_2H_5^+$ is planar, with an absolute minimum corresponding to an oxygen−oxygen separation of $R = 2.37$ Å. At the absolute minimum, there is no barrier opposing the transfer, and the central proton is located halfway between the two water oxygen atoms. As the oxygen−oxygen separation increases, a barrier defining a double well appears and gradually increases in height.

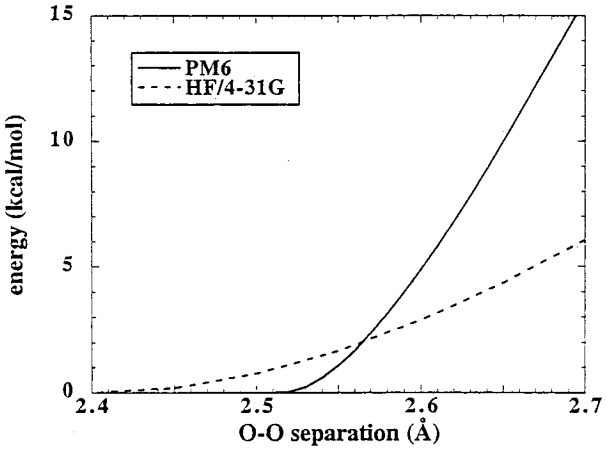

Figure 1. Dependence of the potential energy barrier for H nucleus motion upon the donner−acceptor distance in $H_2O-(H^+)-OH_2$. The results from *ab initio* calculations at the HF/4-31G level (dashed line) and from the PM6 model (solid line) are shown.

Analogous calculations done with the PM6 model indicate that the global minimum on the potential energy surface lies at $R =$ 2.46 Å and corresponds to a C_{2h} geometry, with the central proton lying halfway between the two water oxygen atoms in a single well. At larger separations, a central barrier emerges. The barrier height is shown in Figure 1 as a function of R for both the *ab initio* calculations and the PM6 model. The empirical PM6 potential overestimates both the oxygen−oxygen distance at the absolute minimum and the barrier height at longer hydrogen bond lengths. However, the presence of a barrier and the dependence of its height upon the donor−acceptor separation is qualitatively reproduced with the PM6 model. Furthermore, in the range of strong hydrogen bond lengths analyzed in this work, 2.50−2.60 Å, the potential energy profiles obtained with both methods are comparable.

Discretized Feynman Path Integral. The importance of quantum effects was investigated by exploiting the isomorphism of the discretized Feynman path integral representation of the density matrix with an effective classical system obeying Boltzmann statistics.[22] Only the quantization of the protons was considered, and the oxygens were treated as classical particles. Following the path integral approach, each proton was replaced in the effective classical system by a ring polymer, or necklace, of P fictitious particles with a harmonic spring between nearest neighbors along the ring. The potential energy of the effective classical system is

$$U_{\text{eff}}(\{\mathbf{r}_O\},\{\mathbf{r}_H^{(1)}\},\ldots,\{\mathbf{r}_H^{(P)}\}) = \frac{1}{P}\sum_{p=1}^{P} U(\{\mathbf{r}_O\},\{\mathbf{r}_H^{(p)}\}) + \sum_{i=1}^{N_H}\sum_{p=1}^{P}\frac{1}{2}K_{\text{polymer}}|\mathbf{r}_{H_i}^{(p)} - \mathbf{r}_{H_i}^{(p+1)}|^2 \quad (2)$$

where $\{\mathbf{r}_H^{(p)}\} = \{\mathbf{r}_{H_1}^{(p)},\ldots,\mathbf{r}_{H_{N_H}}^{(p)}\}$ represents the coordinates of the pth particle for protons H_1 through H_{N_H}. The harmonic spring constant acting between the pth and $(p+1)$th nearest neighbors along the polymer necklace representing each proton H_i of mass M_H, is defined as $K_{\text{polymer}} = PM_Hk_BT/\hbar^2$, where k_BT and $\hbar$ are the Bolztmann thermal energy and Planck constant, respectively. In the second summation of eq 2, $\mathbf{r}^{(P+1)} \equiv \mathbf{r}^{(1)}$ is required so as to satisfy the closure of the ring polymers. In the present path integral simulations, each proton was represented as a polymer necklace of $P = 32$ fictitious particles. This choice is appropriate for the present system, as discussed elsewhere.[27]

Langevin Dynamics Simulations. The configurational sampling was performed by generating Langevin molecular dynamics trajectories of the effective system. For all degrees of freedom x_α in the effective classical system, the trajectory was calculated according to the Langevin equation of motion,

$$m_\alpha\ddot{x}_\alpha = -\partial_{x_\alpha}U_{\text{eff}} - \gamma\dot{x}_\alpha + f(t) \quad (3)$$

where γ is a friction constant and $f(t)$ is a random Gaussian force obeying the fluctuation−dissipation theorem,

$$\langle f(t)\, f(0)\rangle = 2k_BT\gamma\delta(t) \quad (4)$$

ensuring that the configurations were generated according to a Boltzmann distribution, $\exp[-U_{\text{eff}}/k_BT]$, at temperature T. It should be emphasized that the resulting Boltzmann distribution is independent of the choice of dynamical mass m_α and friction constant γ attributed to each degree of freedom. The choice of Langevin dynamics was dictated by the need to avoid the nonergodicity of path integral simulations based on molecular dynamics with thermostats.[38]

In the course of the trajectories of the effective system, the full PM6 potential function, $U(\{\mathbf{r}_O\},\{\mathbf{r}_H^{(p)}\})$, was recalculated for each p-step of the discretized path integral. In particular, the interactions involving the pairwise interactions ϕ_{HH} and ϕ_{OH} were recalculated. It is important to note that the induced polarization energy contribution, $\Phi_{\text{pol}}(\{\mathbf{r}_O\},\{\mathbf{r}_H^{(p)}\})$, was calculated self-consistently for each set of polarization vector $\{\boldsymbol{\mu}^{(p)}\}$. In other words, each molecular dynamics time step involved the determination of 32 polarization states induced on the oxygen atoms. The forces on all particles due to the many-body polarization were calculated analytically by solving a similar set of self-consistent equations derived by Stillinger.[30] In contradiction to previous statements,[39] it was verified by finite differentiation that the analytical forces were consistent with the gradient of the PM6 energy. For computational efficiency, contributions arising from constant terms, such as the oxygen−oxygen ϕ_{OO} interaction and the dipole−dipole interaction tensor, were calculated only once and stored.

Molecular dynamics simulations were performed on protonated linear chains of 4 ($O_4H_9^+$), 5 ($O_5H_{11}^+$), and 9 ($O_9H_{19}^+$) water molecules using the method described above. The simulations were repeated in the classical limit, which corresponds to $P = 1$. The energy-optimized conformation of the chain was used as a starting point. During the course of the simulations, a harmonic restoring potential with a force constant of 10 (kcal/mol)/Å^2 was applied to any oxygen atom lying beyond 0.75 Å from the axis of the linear chain. This cylindrical restoring potential was used to model the channel environment of the proton wire and to maintain the linearity of the chain. The trajectories were generated at 300 K with a modified version of the CHARMM program[40] using Langevin dynamics with a time step of 0.5 fs. A dynamical mass corresponding to the mass of a proton was assigned to each p-proton in the ring polymers. A friction coefficient γ corresponding to a velocity relaxation time of 0.2 ps was assigned to all of the particles in the effective system. After equilibration, 2 ns simulations were produced for both the classical and the effective quantum systems. The coordinates of the system were recorded every 100 steps for analysis.

One-Dimensional Schroedinger Equation. To examine the character of the quantization of the proton motion, the energy levels E^n and the corresponding wave functions $\psi_n(r)$ of the central proton in the tetrameric water chain were calculated by solving the one-dimensional Schroedinger equation numerically,

$$-\frac{\hbar^2}{2M_H}\psi_n''(r) + U(r)\,\psi_n(r) = E^n\psi_n(r) \quad (5)$$

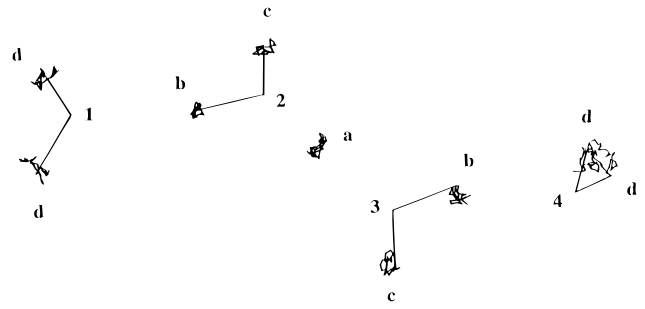

Figure 2. Instantaneous configuration of the protonated water tetramer, $O_4H_9^+$, in the path integral representation. The four oxygen atoms are labeled 1−4, while the ring polymers representing the nine hydrogen nuclei are labeled a−d according to the topological symmetry of the cluster. Note that H_a is shared by O_2 and O_3 in a strong hydrogen bond.

The potential energy profile $U(r)$ was calculated from a given configuration of the chain by moving the central proton along the oxygen−oxygen axis at a distance r from one of the oxygen atoms. All other degrees of freedom were held fixed. Equation 5 was solved numerically by using a basis set constructed from the lowest eigenstates of the particle in a square well potential of width L, namely, functions of $\sin(n\pi r/L)$, where n is a nonzero integer. The potential was assumed to be infinite for $r \leq r_0$ and $r \geq r_0 + L$. The choices of $r_0 = 0.8$ Å, $L = 1.0$ Å, and $1 \leq n \leq 10$ were found to be appropriate for the calculations.

Results and Discussion

Quantum Energy Levels of the Excess Proton. The importance of quantum effects arising from the light mass of the hydrogen nuclei is first investigated in detail in the case of the protonated tetrameric water chain. Figure 2 shows a statistically representative configuration of the system in the path integral representation. The ring polymers corresponding to each hydrogen nucleus are depicted, and each O−H covalent bond is drawn between the oxygen and the first bead of each path integral necklace. On average the central hydrogen bond is much stronger than the two outlying hydrogen bonds. As reported in a previous publication,[27] the central proton is located halfway, on average, in the strong hydrogen bond between oxygen atoms 2 and 3 in the $O_4H_9^+$ chain. The quantum dispersion of the hydrogen nuclei results in an average spread of the ring polymers over 0.28−0.30 Å, whereas the De Broglie wavelength of hydrogen nuclei is closer to 0.5 Å. The reduction reflects the confinement of chemical O−H bonds.[27]

Because the height of the barrier opposing the motion of proton between two water molecules is strongly dependent upon the donor−acceptor separation (see the preceding section), a proton involved in a strong hydrogen bond is more likely to undergo transfer than a proton in a comparatively weaker hydrogen bond. Our previous study showed that the central hydrogen bond is the strongest on average, with donor−acceptor separations covering a range of cases in which the barrier to proton transfer is moderate, small, or vanishing.[27] For this reason, we focus on the central hydrogen nucleus of $O_4H_9^+$. For examination of the character of the quantum mechanical state of the central proton, the properties of 300 configurations selected randomly from the path integral simulation were analyzed in detail. For each of these configurations, the potential energy $U(r)$ for the motion of the central proton was computed as a function of the O−H separation r in the fixed field of the other nuclei. From each potential energy profile thus obtained, the quantum energy levels E^n and the corresponding wave functions $\psi_n(r)$ of the central proton were calculated by solving the one-dimensional Schroedinger equation numerically. The energies of the ground and first excited states

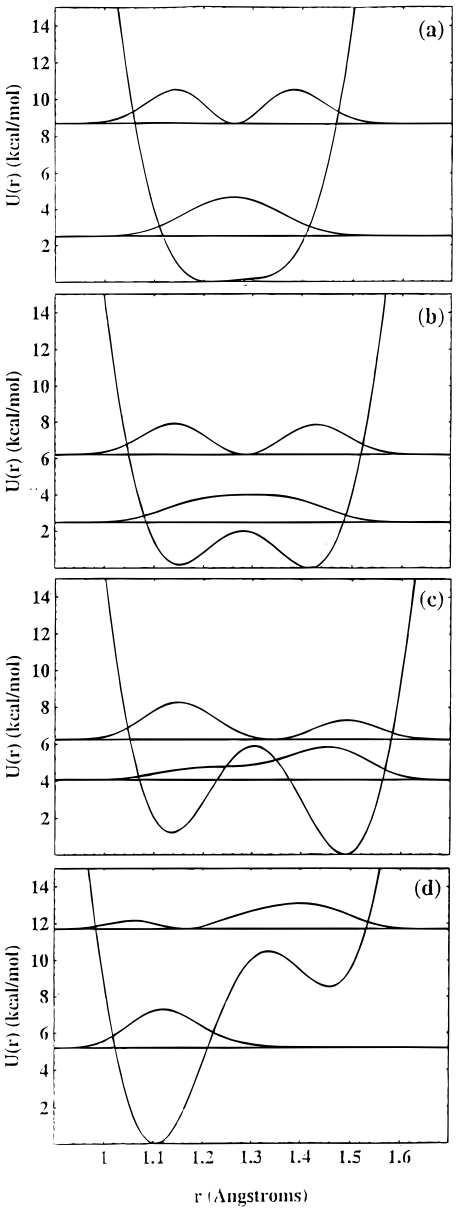

Figure 3. Potential energy profiles for the motion of an excess proton in a linear water tetramer calculated from an MD trajectory at 300 K. The zero point and first excited states of the proton are shown, together with the probability densities $||\psi_0(r)||^2$ and $||\psi_1(r)||^2$, in four examples: (a) no barrier to proton transfer; (b) smaller barrier lower than the zero point energy; (c) proton tunneling; (d) strong symmetry. The four distinct classes correspond respectively to 59, 27, 11, and 3% of the configurations sampled at 300 K. The results were obtained by solving eq 5 numerically.

of the central proton, respectively, E^0 and E^1, the barrier height, $E^{\ddagger}$, and the energy splitting between reactant and product wells, ΔE, were defined relative to the absolute minimum of the potential $U(r)$. The interplay of the proton's vibrational energy with the potential energy profile for motion along the tetramer's central hydrogen bond is illustrated in Figure 3. Four cases, corresponding to increasingly weak hydrogen bonds, can arise. In the first case (a), the oxygen−oxygen distance is short and there is no intrinsic barrier to proton transfer ($E^{\ddagger} = \Delta E = 0$); in the second case (b), there is a barrier which is lower than the zero point energy of the proton ($E^{\ddagger} \leq E^0$); in the third case (c), the ground state wave function occupies the classically-forbidden region of the central barrier ($\Delta E \leq E^0 < E^{\ddagger}$); and finally, in the fourth case (d), the ground state distribution of the proton is confined to one well due to the strong asymmetry of the potential ($\Delta E > E^0$).

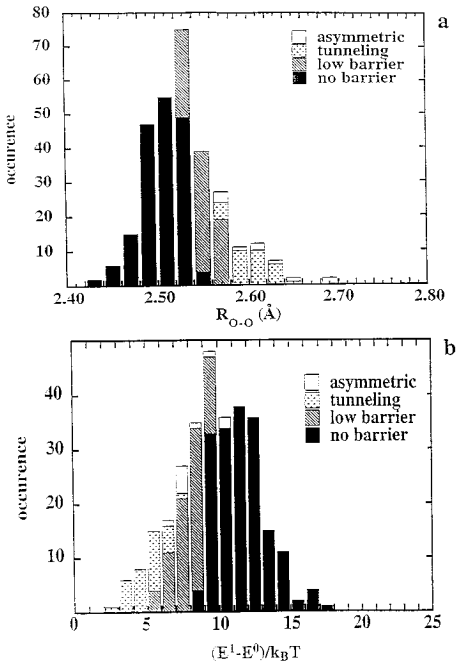

Figure 4. Distribution of O−O distances for the central hydrogen bond in $O_4H_9^+$ (a) and distribution of first vibrational excitation energies for the central proton of $O_4H_9^+$ (b).

The four distinct classes a−d defined above correspond respectively to 59, 27, 11, and 3% of the configurations sampled at 300 K. Configurations in which the central proton is strongly bound to a single water molecule (case d) are infrequent. Configurations in which the proton is shared by the two central water molecules without a significant energy barrier (case a or b) occur 86% of the time. Lastly, we note that in the third class (c), the ground state wave function is delocalized over both wells, indicating that proton tunneling through the barrier can occur.[14] Conditions favorable to proton tunneling prevail 11% of the time. As we shall see, this corresponds to a relatively symmetric double well and a low first-excitation energy.

Histograms for the distribution of the O_2-O_3 separation are shown in Figure 4a. This distance is seen to vary very significantly over the course of the simulation, from 2.43 to 2.70 Å, under the influence of thermal fluctuations. Because the energy profile for the motion of the central proton is very sensitive to the O_2-O_3 separation, configurations in which the barrier is alternatively moderate, small, or absent occur spontaneously. The four cases described above are distinguished in Figure 4a. The case where there is no barrier (a) dominates up to O_2-O_3 separations of 2.54 Å, whereas separations of 2.58 Å and more correspond exclusively to tunneling and strong asymmetry conditions, c and d. Interestingly, the strong asymmetry in d arises from atypical configurations where one of the end hydrogen bonds in the tetramer (i.e., either O_1-O_2 or O_3-O_4) is stronger than O_2-O_3. Compared to the statistically dominant cases, the asymmetric case corresponds to configurations where the central proton is not shared by two water molecules and where transfer has effectively occurred. These results illustrate the flexibility of the system and how the localization of the central proton is affected by variations in the geometry of the hydrogen-bonded chain as a whole (thermal effects).

An important question is that of the dominance of the ground state of the proton. Figure 4b depicts the histogram of the distribution of first excitation energies in units of thermal energy k_BT. Clearly, in most cases, the energy required to reach excited vibrational states is significantly larger than the thermal energy.

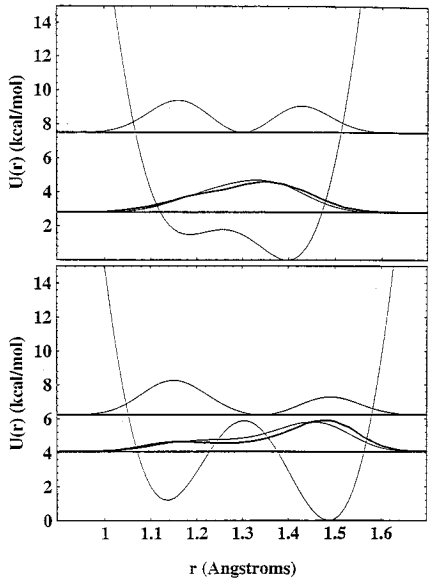

Figure 5. Two examples for the comparison of the proton distributions along the central hydrogen bond of $O_4H_9^+$. The probability densities $||\psi_0(r)||^2$ and $||\psi_1(r)||^2$ calculated from the solution of the one-dimensional Schroedinger equation (thin) and the density matrix obtained from the path integral treatment (bold) are shown.

A notable exception arises at the lower end of the distribution, in which the excitation energy is comparable to the thermal energy. Figure 4b shows that this condition corresponds to case c, where the proton can tunnel through the potential energy barrier. To further illustrate the ground state dominance, we compare the probability density of the ground state and the first excited state obtained from the solution of the one-dimensional Schroedinger equation, $||\psi_0(r)||^2$ and $||\psi_1(r)||^2$, with the average spatial distribution of the central proton obtained from a 10 ps path integral simulation of the tetrameric system in which all of the other nuclei were held fixed. The results are shown in Figure 5. First, we note (with some satisfaction) that the results obtained with these two significantly different methods are remarkably consistent with each other. In both examples shown, the projection of the thermally averaged path integral proton distribution along the hydrogen bond axis is seen to closely resemble the analytical ground state probability density. However, contributions from excited states are required to recover the finite-temperature path integral distribution. This is especially true in the case depicted at the bottom of Figure 5, because the first excitation energy is in the low-lying limit for this configuration. Since the first excitation energy is generally larger than k_BT, the properties of the system are dominated by the ground state wave function of the proton. A similar conclusion was reached in a previous study of small proton hydrates by considering the complex time correlation function, $C(p,p') = \langle(\mathbf{r}_{H_i}^{(p)} - \mathbf{r}_{H_i}^{(p')})^2\rangle$.[26] The present analysis shows that the ground state is less dominant for some configurations in which the central proton is delocalized over a relatively symmetric double-well potential (class c).

For further analysis of the character of quantum effects in relation to the geometry of the hydrogen-bonded chain, the distribution of the first excitation energy, E^1-E^0, was plotted as a function of the zero point energy, E^0. The result is shown in Figure 6. In this scatter plot, different symbols were used according to the four cases described above. The four cases correspond to well-defined regions of the (E^0, $E^1 - E^0$) map. In the strong asymmetry case (d), the proton is confined to the well lowest in potential energy. In that well, the first vibrational excitation energy is comparable to the zero point energy: i.e., $E^1 - E^0 \simeq E^0$ (circles in Figure 6). On the contrary, tunneling conditions (case c) are met with a nearly symmetric double well,

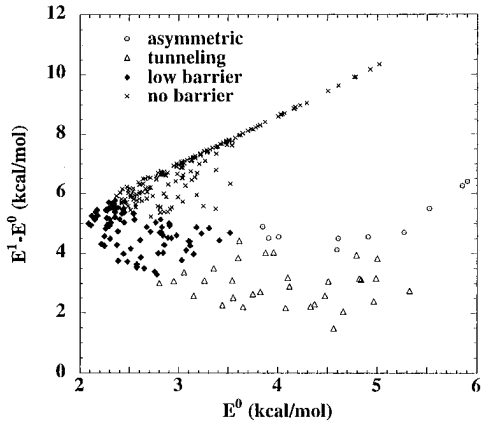

Figure 6. Distribution of properties of the central H^+ of $O_4H_9^+$ as a function of its zero point and first excitation vibrational energies.

which corresponds to a small first excitation energy (shown with triangles at the bottom of Figure 6). As the donor−acceptor separation decreases, the barrier is lowered and becomes less than the zero point energy (case b) and eventually vanishes (case a). The anharmonicity gives rise to a very flat well. Such broad wells appear both in regions of small E^0 and of large $E^1 - E^0$. As the single well gets narrower due to a shorter O−O separation, the vibrational energy of the proton increases. There is a linear dependence with a slope of approximately 1.75 between the first excitation energy and the zero point energy in case a. A slope of 2 would be observed if the energy levels corresponded to those of a harmonic well with variable vibrational frequency ω and were exactly given by $E^n = (1/2 + n)\hbar\omega$. It is important to note that the zero point energy undergoes significant variations, from 2 to 6 kcal/mol, which may have important effects on the accessible configurations of the system.

Proton−Proton Correlations. As the previous analysis demonstrates, the motion of the central proton is strongly coupled to the configuration of the chain of water molecules in the $O_4H_9^+$ system. This raises important questions concerning the presence of collective motions and the importance of quantum correlations between the different hydrogen nuclei in the system. In order to address such questions, the quantum correlation coefficients C_{H_i,H_j} between two distinct ring polymers H_i and H_j were estimated as

$$C_{H_i,H_j} = \frac{\left\langle \frac{1}{P}\sum_{p=1}^{P} (\mathbf{r}_{H_i}^{(p)}(t) - \bar{\mathbf{r}}_{H_i}(t))(\mathbf{r}_{H_j}^{(p)}(t) - \bar{\mathbf{r}}_{H_j}(t)) \right\rangle}{R_{H_i}^{gyr} R_{H_j}^{gyr}} \quad (6)$$

where

$$R_{H_i}^{gyr} = \left\langle \frac{1}{P}\sum_{p=1}^{P} |\mathbf{r}_{H_i}^{(p)}(t) - \bar{\mathbf{r}}_{H_i}(t)|^2 \right\rangle^{1/2} \quad (7)$$

is the radius of gyration of ring polymer H_i and $\bar{\mathbf{r}}_{H_i}(t) = 1/P\sum_{p=1}^{P}\mathbf{r}_{H_i}^{(p)}(t)$ corresponds to the position of the centroid of ring polymer H_i at time t. Table 1 lists the normalized quantum cross-correlation coefficients between the *p*-protons on second-neighbor polymer rings, as calculated from eq 6. In the event of full correlation, the position of each *p*-proton relative to the centroid would be identical to that of the corresponding *p*-proton in the other polymer ring, and the value of that coefficient would be exactly 1. Inversely, a coefficient of −1 would indicate strong anticorrelation, whereby the position of each *p*-proton relative to the centroid would be diametrically opposed to that of the corresponding *p*-proton in the neighboring polymer ring. As Table 1 shows, the average quantum correlation coefficients are all negative, as the charge−charge repulsion between individual protons favors anticorrelation between the ring polymers. The coefficients are also relatively small, ranging from -5×10^{-3} to -4×10^{-2}. For comparison, the value extracted from a test simulation of two hydrogen nuclei whose centroids were forced to lie at the origin is −0.95. The correlation drops to −0.122 if the centroids are separated by 2 Å and to −0.026 when the separation is 20 Å. A value of -4×10^{-2} was obtained for the cross-correlation coefficient of the two hydrogen nuclei in an isolated water molecule. This value is consistent with that obtained for the hydrogens of each of the individual water molecules 1−4 in $O_4H_9^+$ (see pairs (*b*,*c*) and (*d*,*d*) in Table 1). Smaller values are obtained for cross-correlation coefficients involving the central hydrogen nucleus H_a. The smallest coefficient shown in Table 1 corresponds to cross correlation between protons *a* and *b*, which are both involved in water−water hydrogen bonds, and to protons *b* and *d*, which are not bound to the same water molecule. The coefficients not listed, which correspond to pairs involving more distant neighbors, are not significant.

TABLE 1: Quantum Mechanical Cross-Correlation Coefficients between First-Neighbor Hydrogen Atoms (See Text), Averaged over 2 ns of Langevin Dynamics of the Protonated Water Tetramer[a]

	H_b	H_c	H_d
H_a	−0.005	−0.01	−
H_b	−	−0.04	−0.005
H_d		−	−0.04

[a] Atomic labels are given in Figure 2.

These results indicate that the quantum correlations between second-neighbor protons are small and somewhat screened by the presence of intervening oxygen atoms. The small magnitude of proton−proton correlations suggests that the density matrix of the hydrogen nuclei in the fixed field of the heavy nuclei could be written as an independent product of effective one-particle distribution functions,

$$\langle \rho_{\{\mathbf{r}_O\}}(\{\mathbf{r}_H\})\rangle \simeq \prod_{i=1}^{N_H} \langle \rho_{\{\mathbf{r}_O\}}(\mathbf{r}_{H_i})\rangle \quad (8)$$

by analogy with the neglect of electron−electron correlations in self-consistent field Hartree−Fock *ab initio* calculations. Using a density matrix of the form given by eq 8 yields proton−proton correlations that are identically zero. A similar approximation could perhaps be useful to describe the real-time dynamics of proton transfer. In a further effort to simplify the description of the system, quantization of the hydrogen nuclei removed from the immediate vicinity of the excess proton may be taken into account solely in terms of reorientational librational motions of water molecules, as suggested by the significant stiffness of OH bonds in water.[41]

Potential of Mean Force. Potential of mean force surfaces (PMF) for the motion of a proton in relation to donor−acceptor separations were calculated with classical and path integral simulations to further understand the mechanism of proton translocation along a linear water chain. The top part of Figure 7 shows the calculated PMF $W(r,R)$, where r and R correspond respectively to the O−H and O−O (donor−acceptor) distances of the central hydrogen bond in the tetrameric water chain. The motion of a classical proton in the tetramer is confined to three wells. The absolute minimum corresponds to a short hydrogen bond at $R = 2.46$ Å, whereas two equivalent, secondary free energy wells exist at $R = 2.60$ Å, which correspond to

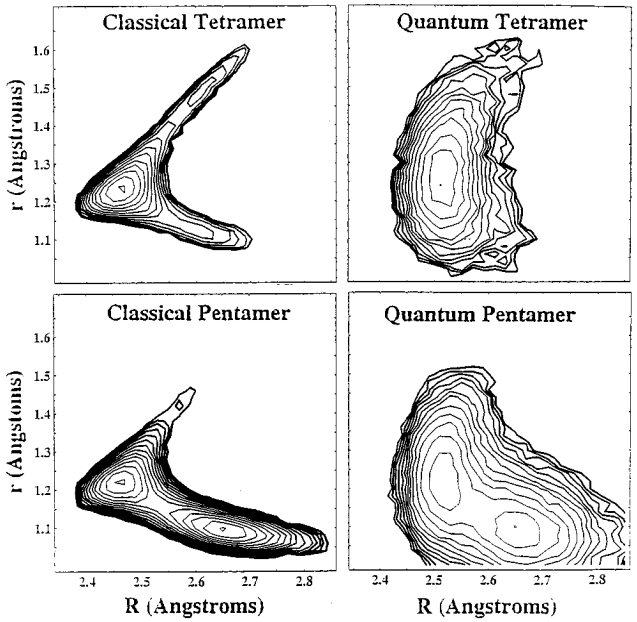

Figure 7. Classical and quantum potential of mean force (PMF) surfaces for the central O−H distance, *r*, as a function of central O−O separation, *R*, in tetrameric and pentameric water chains.

configurations where the central proton is bound to one of the two surrounding water oxygen atoms. In sharp contrast, the PMF contours in the path integral quantum treatment indicate that the central proton is largely delocalized over a single broad well with an absolute minimum at $R = 2.52$ Å, which englobes the configurations corresponding to the classical secondary minima. In general, the zero point energy of the proton is sufficient for overcoming the moderate potential energy barrier opposing the transfer at short O−O separations. Consequently, all the configurations obtained at thermal equilibrium correspond to a single minimum in the PMF mapped along central O−H separations.

For examination of the influence of increasing the length of the hydrogen bonded chain, the corresponding PMF's were also calculated from classical and quantum simulations for the hydrogen bonds involving the central oxygen atom of the pentameric chain, $O_5H_{11}^+$. The bottom half of Figure 7 shows the calculated PMF's for the pentameric chain. In this case, *R* and *r* designate the O−O and O−H distances for either hydrogen bond involving the central oxygen atom. As in the tetrameric chain, three minima are observed in the classical limit. But, in contrast to the previous case, the minima are distinguished by a strong asymmetry in the pentamer. The global minimum at $R = 2.65$ Å corresponds to a moderately strong hydrogen bond with a covalently bound H at $r = 1.10$ Å. In such configurations, the underlying potential energy profile for the motion of a hydrogen nucleus is strongly asymmetric, whereby the proton is closely associated with the central oxygen atom. The free energy well corresponding to a strong hydrogen bond at $R = 2.47$ Å is also found, merely 0.2 kcal/mol higher in energy. In addition, the third free energy well in the classical pentamer PMF lies 2.6 kcal/mol above the global minimum at $(R,r) =$ (2.57 Å, 1.43 Å) and corresponds to infrequent configurations in which, instead of the central water molecule, it is one of the off-central water molecules which is covalently bound to H^+. Compared to the tetramer, in the pentamer the symmetry of the PMF profile has been broken by the addition of a water molecule at one end of the chain. Nevertheless, the quantum treatment of protons has a similar effect in the tetrameric and pentameric chains (see Figure 7). Compared to their classical counterparts, the wells of the PMF broaden dramatically due to the vibrational energy and tunneling of the hydrogen nuclei along the hydrogen

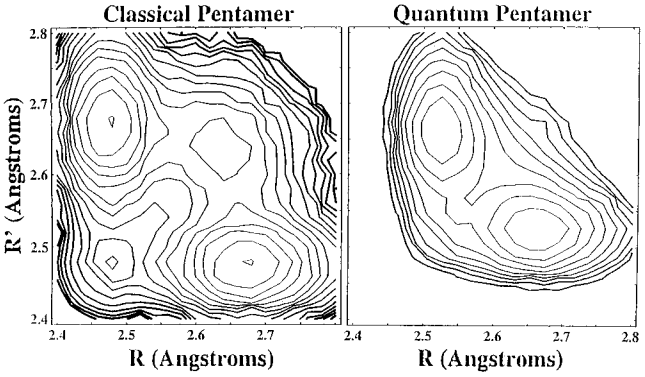

Figure 8. Classical and quantum PMF surfaces for the two O−O separations involving the central water molecule of $O_5H_{11}^+$.

bonds lying on either side of the central oxygen atom. The two lowest minima subsist and possess approximately the same free energy.

In Figure 8 the classical and quantum PMF surfaces $W(R,R')$, where *R* and *R*′ designate the off-central oxygen−oxygen distances in the pentamer, are depicted. The classical PMF contours delineate four minima corresponding to (long, short), (short, long), (long, long) and (short, short) configurations of hydrogen bonds 2 and 3 of the chain. The configurations corresponding to the two asymmetric minima, (short, long) and (long, short), are lowest in free energy. The other two minima on the classical surface are shallow. They lay respectively 0.7 and 1.2 kcal/mol higher in energy and correspond to a "hydronium-like" structure involving symmetric configurations of the heavy atoms. In the classical limit, the exchange between (short, long) and (long, short) configurations of the system takes place via such symmetric, hydronium ion intermediate states. In the quantum treatment, there are only two stable configurations, for which one of the hydrogen bonds is short at 2.52 Å and the other is long at 2.68 Å, with a free energy barrier of only 0.6 kcal/mol between them, compared to 0.9 and 1.4 kcal/mol in the classical limit.

The above results indicate how the geometry and the length of the chain, combined with thermal fluctuations, participate in the proton translocation mechanism. In the pentameric water chain, as in the tetramer, there is in general only one short, strong hydrogen bond in a given configuration. The size and asymmetry of the two chain segments lying on either side of the strong hydrogen bond have a determining influence on the free energy for the translocation of the excess proton along the water chain. In the tetramer, the potential energy profile does not often deviate very much from a symmetric configuration because of the limited size of the chain. Therefore, there is no substantial potential energy barrier along this strong hydrogen bond, and with the help of zero point energy, the delocalization of the hydrogen nucleus from one water molecule to the other prevails statistically. Such properties correspond to a "nonpolar" hydrogen bond in the sense of Zundel (symmetric charge distribution in $O-H^+-O$).[42] By contrast, with the addition of an extra water molecule to form the pentamer, the intrinsic energy profile for proton motion along the strong hydrogen bond becomes asymmetric, or "proton-polarized". From the PMF we learn that while the excess (transferring) proton is in general confined to the central hydrogen bond of the tetrameric chain, isomerization around the central OH_2 of the pentameric chain can readily take place at 300 K. The translocation mechanism is sensitive to variations in the geometry of the proton wire as a whole.

The above results also indicate that the quantum nature of the hydrogen nuclei affects the equilibrium configuration of the heavy atoms at the center of the system significantly. Further-

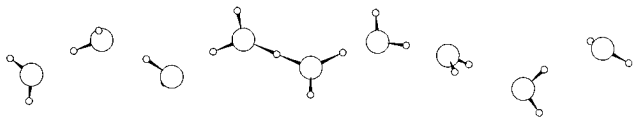

Figure 9. Classical representation of the linear chain of 9 hydrogen-bonded water molecules with one excess proton.

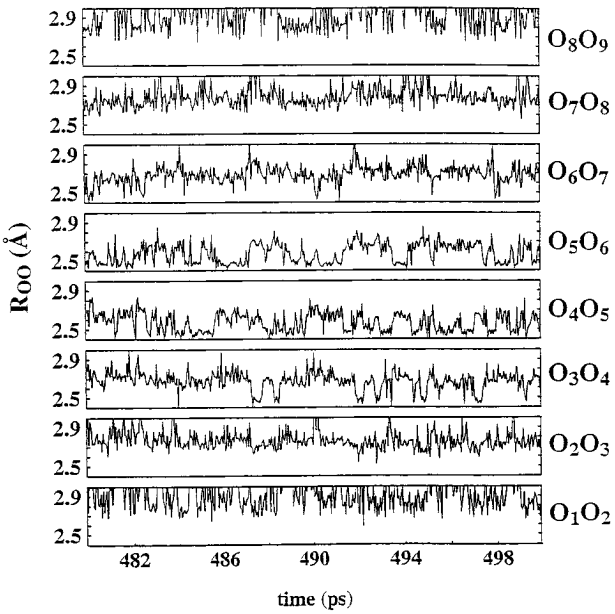

Figure 10. Time evolution of the distances between adjacent oxygen atoms in a protonated chain of 9 hydrogen-bonded water molecules.

more, a lower PMF barrier suggests that the interconversion between the two limiting structures of the pentamer is facilitated by the inclusion of quantum effects. Yet, because the interconversion occurs via the formation of $O_2H_5^+$ in both the quantum and classical cases, we note that the changes in heavy atom configuration coupled to proton translocation along the chain are similar in both treatments and do not differ fundamentally.

Proton Mobility along a Chain of Nine Water Molecules. In this section we further investigate the mechanism of proton mobility along a chain of 9 water molecules. Classical simulations were used ($P = 1$), because the discretized path integral treatment is valid only for calculating average properties from the equilibrium density matrix and does not allow one to follow the real-time dynamics of the system. On the basis of the preceding analysis, it is reasonable to expect that the classical limit can provide meaningful insight into the molecular mechanism governing proton transfer.

The protonated nonamer is shown in Figure 9. As was observed with a pentameric water chain, it is the central water molecule that binds the excess proton most often. On average, the hydrogen bonds involving the central oxygen are strongest, with the remaining hydrogen bonds in the chain getting progressively weaker with increasing distance from the center. By following the dynamics of the oxygen−oxygen distances along the chain, we focus on the degrees of freedom that appear to be strongly coupled to the transfer of proton. In Figure 10, the successive O−O separations are shown as a function of time for a 20 ps window. These data, which were extracted from a 2 ns simulation of $O_9H_{19}^+$, help characterize the dynamics of the chain. While the four outer hydrogen bonds remain weak at all times, the four central hydrogen bonds are seen to become alternatively long and short. At any given time, one of them is shorter than the others, at $R \simeq 2.50$ Å. In contrast, the other O−O distances range from 2.65 Å all the way to 2.9 Å (at the edges of the oligomer). The location of the strong hydrogen bond is chaotic and fluctuating rapidly. From Figure 9, the lifetime of a strong hydrogen bond in the chain is seen to vary from 0.05 ps or less, up to periods of approximately 1 ps. On the basis of the analysis of the mean-square fluctuations of the strong hydrogen bond over the entire simulation of 2 ns, the position of the excess proton diffuses from one O−O pair to the adjacent one at an estimated rate of 1.2 ps^{-1}. This interchange takes place via large variations in O−O separations. For instance, the O_4-O_5 distance remains short for 1 ps around $t \simeq 485$ ps (Figure 9). Then, there is a large fluctuation which is anticorrelated with strengthening of O_5-O_6. That hydrogen bond remains strong for about 1.5 ps, until large successive fluctuations take the excess proton transiently back through O_4-O_5 to O_3-O_4 ($t \simeq 487$ ps). A detailed observation of Figure 10 reveals that such large fluctuations are accompanied by smaller, opposite changes in the O−O separations of neighboring hydrogen bonds. Thus, the mechanism of proton translocation emerges as a cooperative dynamical process involving more than just 2 or 3 water molecules. Occasionally, collective motions may favor a rapid propagation of the process over several hydrogen bonds within less than 1 ps (see the diffusion from O_6-O_7 to O_3-O_4 between $t = 491$ and 492 ps). There are also many recrossings, which indicates that the translocation process is strongly non-Markovian. This last observation warrants the modelization of proton wires using a master equation.[43]

Compared to the pentameric water chain, the net mobility of protons along the nonamer is very notably enhanced. This may be described as a "solvent effect", whereby the proton translocation is ultimatey driven by fluctuations in the polar environment. In hydrogen-bonded chains of finite size, the excess charge is best solvated at the center of the chain. As the length of the chain increases, the transfer of protons along more distant, off-central hydrogen bonds is made increasingly accessible by the relative stabilization of asymmetric configurations of the chain's heavy atom. All hydrogen bonds become equivalent in the limit of an infinite chain. In that perspective, the above results suggest that changes in the relative strength of hydrogen bonds constitute the rate limiting step for the net diffusion of the proton transfer reaction in a long hydrogen-bonded chain.

In the future, the necessity to characterize and follow the dynamical translocation of protons along long chains of water molecules could raise the need for a collective reaction coordinate that takes into account the asymmetry (or proton polarity) of the hydrogen bonded chain. Since the distance between nearest oxygen neighbors is a dominant factor governing the proton translocation, we propose constructing a reaction coordinate $\mathbf{r}$ as a weighted average over oxygen−oxygen distances,

$$\mathbf{r} = \sum_{i,j} \frac{(\mathbf{r}_{O_i} + \mathbf{r}_{O_j})}{2} \left[\frac{w(|\mathbf{r}_{O_i} - \mathbf{r}_{O_j}|)}{\sum_{k,l} w(|\mathbf{r}_{O_k} - \mathbf{r}_{O_l}|)} \right] \tag{9}$$

where $w(r)$ is a smooth weighting function designed to give more statistical weight to strong hydrogen bonds; e.g., $w(r)$ is equal to 1 when the O−O distance is less than 2.60 Å, and close to zero when it is larger. Such a construction would allow the analysis of a long-time correlation function describing proton translocation along a linear chain as well as in bulk solution.

Conclusions

In this work, we have characterized the properties of proton wires and provided some insight into the complex interplay

governing the molecular mechanism of H^+ translocation in hydrogen-bonded chains. Although proton transfer reactions in model systems are sometimes distinguished on the basis of the strength of the hydrogen bond, the distinction is not appropriate in the case of protonated water chains. This is because, in such flexible systems, the presence of an excess proton forces the range of thermally-accessible water−water separations to include moderate and strong hydrogen bonds, for which the energy barriers vary from fairly large to small, and often vanish. Thus, the flexibility of water hydrogen bonds with an excess proton, combined with zero point energy effects, is essential in modulating the process leading to proton translocation. Furthermore, the polar, protic nature of the whole system underlines the importance of collective properties.

All the relevant effects were incorporated in the present model, and the interdependence of quantum effects with the geometry of the water−water hydrogen bond was analyzed in some detail. The motion of protons appears to be dominated by the ground state nuclear wave function, and the influence of quantum effects on the local geometry of the proton wire was seen to be significant. Cross-correlation coefficients between protons seem negligible, suggesting that the density matrix of the hydrogen nuclei is separable into an independent product. The sharing of an excess proton by two water molecules engaged in a strong hydrogen bond dominates in a nearly symmetric environment; breaking that symmetry favors the thermal interconversion of structures in which a proton is shared alternatively by neighboring pairs of water molecules. Moreover, our results suggest that the rate limitation for translocation over several hydrogen bonds arises from successive thermal fluctuations involving the heavy nuclei of the entire chain. Thus, while the mechanism for proton transfer can be rationalized from the properties of hydrogen bonds between two water molecules, the net translocation of H^+ is governed by symmetry-breaking effects arising from cooperative motions within the water chain at large.

It is interesting to compare the present results with proposed mechanisms for the transport of protons in liquid water. As noted in the recent report of an *ab initio* simulation of H^+ in bulk water,[21] it is the reorganization of water molecules in the solvation shell of OH_3^+ and $O_2H_5^+$ that limits the rate of translocation in three dimensions. The reason is that the coordination number of OH_3^+ (three) differs from that of H_2O (four) in bulk water.[21] In contrast, the coordination of water molecules (besides the extrema) is always two along a linear water chain, and the proton transfer coordinate is modulated by subtle effects involving the relative strength of pre-existing hydrogen bonds. Moreover, in linear water chains the "solvated proton" is more akin to $O_2H_5^+$ than to OH_3^+. On the basis of these observations, a reaction coordinate was proposed to follow the dynamics of proton translocation.

While this study was restricted to protonated water chains in vacuo, it should have interesting implications for the transport of protons along biological water wires, where additional perturbations to the symmetry of the water chain are likely to arise from the presence of charges or other hydrogen-bonding competitors. Moreover, the polarization properties of water molecules will change in the presence of a membrane potential. These factors should affect the energy profile for proton translocation and the dynamics of the proton wire. In that perspective, the extension of the present methodology to studies of proton wires embedded in complex biological systems has been undertaken in our laboratory.[31]

Acknowledgment. This work was supported by a grant from the Medical Research Council of Canada. B.R. is a FRSQ research fellow.

References and Notes

(1) Stryer, L. *Biochemistry*; W. H. Freeman and Co.: New York, 1988.
(2) Cao, Y.; Váró, G.; Chang, M.; Ni, B.; Needleman, R.; Lanyi, J. K. *Biochemistry* **1991**, *30*, 10972−10979.
(3) Baciou, L.; Michel, H. Submitted for publication in *Biochemistry*.
(4) Martinez, S. E.; Cramer, W. A.; Smith, J. L. Communication at the 39th Annual Biophysical Society Meeting, San Francisco, 12−16 Feb 1995. Abstract published in: *Biophys. J.* **1995**, *68*, A246.
(5) Papadopoulos, G.; Dencher, N.; Zaccaï, G.; Büldt, G. *J. Mol. Biol.* **1990**, *214*, 15−19.
(6) Henderson, R.; Baldwin, J. M.; Ceska, T. A.; Zemlin, F.; Beckmann, E.; Downing, K. H. *J. Mol. Biol.* **1990**, *213*, 899−929.
(7) Zhou, F.; Windemuth, A.; Schulten, K. *Biochemistry* **1993**, *32*, 2291−2306.
(8) Nagle, J. F.; Morowitz, H. J. *Proc. Natl. Acad. Sci. U.S.A.* **1978**, *75*, 298−302.
(9) Hille, B. *Ionic Channels of Excitable Membranes*; Sinauer Associates Inc.: Sunderland, MA, 1992.
(10) Roux, B.; Karplus, M. *Annu. Rev. Biophys. Biomol. Struct.* **1994**, *23*, 731−761.
(11) Nagle, J. F. *J. Bioener. Biomembr.* **1987**, *19*, 413−426.
(12) Akeson, M.; Deamer, D. W. *Biophys. J.* **1991**, *60*, 101−109.
(13) Borgis, D. In *Electron and Proton Transfer in Chemistry and Biology*; Müller, A., Ratajczak, H.; Junge, W.; Diemann, E., Eds.; Elsevier: Amsterdam 1992.
(14) Borgis, D.; Hynes, J. T. In *The Enzyme Catalysis Process*; Cooper, A., Houben, J. L., Chien, L. C., Eds.; Plenum Publishing Corp.: London, 1989.
(15) Laria, D.; Ciccotti, G.; Ferrario, M.; Kapral, R. *J. Chem. Phys.* **1992**, *97*, 378−388.
(16) Borgis, D.; Tarjus, G.; Azzouz, H. *J. Chem. Phys.* **1992**, *97*, 1390−1400.
(17) Tortonda, F. R.; Pascual-Ahuir, J.-L.; Silla, E.; Tuñón, I. *J. Phys. Chem.* **1993**, *97*, 11087−11091.
(18) Ando, K.; Hynes, J. T. In *Structure, Energetics and Reactivity in Aqueous Solution*; Cramer, C. J., Truhlar, D. G., Eds.; American Chemical Society: Washington, DC, 1994.
(19) Komatsuzaki, T.; Ohmine, I. *Chem. Phys.* **1994**, *180*, 239−269.
(20) Corongiu, G.; Kelterbaum, R.; Kochanski, E. *J. Phys. Chem.* **1995**, *99*, 8038−8044.
(21) Tuckerman, M.; Laasonen, K.; Sprik, M.; Parrinello, M. *J. Phys. Chem.* **1995**, *99*, 5749−5752.
(22) Chandler, D.; Wolynes, P. G. *J. Chem. Phys.* **1981**, *74*, 4078−4095. Zheng, C.; Wong, C. F.; McCammon, J. A.; Wolynes, P. G. *Chim. Scr.* **1989**, *29A*, 171−179.
(23) Lobaugh, J.; Voth, G. A. *Chem. Phys. Lett.* **1992**, *198*, 311−315.
(24) Lobaugh, J.; Voth, G. A. *J. Chem. Phys.* **1994**, *100*, 3039−3047.
(25) Laria, D.; Ciccotti, G.; Ferrario, M.; Kapral, R. *Chem. Phys.* **1994**, *180*, 181−189.
(26) Cheng, H.-P.; Barnett, R. N.; Landman, U. *Chem. Phys. Lett.* **1995**, *237*, 161−170.
(27) Pomès, R.; Roux, B. *Chem. Phys. Lett.* **1995**, *234*, 416−424.
(28) Weber, T. A.; Stillinger, F. H. *J. Phys. Chem.* **1982**, *86*, 1314−1318.
(29) Stillinger, F. H.; David, C. W. *J. Chem. Phys.* **1978**, *69*, 1473−1484.
(30) Stillinger, F. H. *J. Chem. Phys.* **1979**, *71*, 1647−1651.
(31) Pomès, R.; Roux, B. Submitted for publication.
(32) Rahmouni, A.; Kochanski, E.; Wiest, R.; Wormer, P. E. S.; Langlet, J. *J. Chem. Phys.* **1990**, *93*, 6648−6653.
(33) Kozack, R. E.; Jordan, P. C. *J. Chem. Phys.* **1992**, *96*, 3131−3136.
(34) Zhu, S.-B.; Singh, S.; Robinson, G. W. *J. Chem. Phys.* **1991**, *95*, 2791−2799.
(35) Frisch, M. J.; Head-Gordon, M.; Trucks, G. W.; Foresman, J. B.; Schlegel, H. B.; Raghavachari, K.; Robb, M. A.; Binkley, J. S.; Gonzalez, C.; Fox, D. J.; Whiteside, R. A.; Seeger, R.; Melius, C. F.; Baker, J.; Martin, R. L.; Kahn, L. R.; Stewart, J. J. P.; Topiol, S.; Pople, J. A. Gaussian, Inc.: Pittsburgh, PA, 1990.
(36) Scheiner, S. *Acc. Chem. Res.* **1985**, *18*, 174−180.
(37) Frisch, M. J.; Del Bene, J. E.; Binkley, J. S.; Schaeffer, H. F., III. *J. Chem. Phys.* **1986**, *84*, 2279−2289.
(38) Allen, M. P.; Tildesley, D. J. *Computer Simulations of Liquids*; Clarendon Press: Oxford, U.K., 1987.
(39) Halley, J. W.; Rustad, J. R.; Rahman, A. *J. Chem. Phys.* **1993**, *98*, 4110−4119.
(40) Brooks, B. R.; Bruccoleri, R. E.; Olafson, B. D.; States, D. J.; Swaminathan, S.; Karplus, M. *J. Comput. Chem.* **1983**, *4*, 187−217.
(41) Kuharski, R. A.; Rossky, P. J. *J. Chem. Phys.* **1985**, *82*, 5164−5177.
(42) Brzezinski, B.; Zundel, G.; Krämer, R. *J. Phys. Chem.* **1987**, *91*, 3077−3080.
(43) Knapp, E.-W.; Schulten, K.; Schulten, Z. *Chem. Phys.* **1980**, *46*, 215−229.

JP9525752